applied sciences

MDPI

*Article*

# Energy Minimization of New Robotic-Type Above-Knee Prosthesis for Higher Battery Lifetime

**Mucahit Ege [1,2,*] and Serdar Kucuk [2]**

[1] Biomedical Device Technology, Gedik Vocational School, Istanbul Gedik University, 34913 Istanbul, Türkiye
[2] Department of Biomedical Engineering, Umuttepe Campus, Kocaeli University, 41380 Kocaeli, Türkiye; skucuk@kocaeli.edu.tr
* Correspondence: mucahit.ege@gedik.edu.tr

**Abstract:** In this paper, an optimization problem for the energy minimization of a new robotic-type three-axes above-knee prosthesis is carried out based on the actuator power consumption. The optimization problem aims to find the optimal link masses with which to minimize the electrical energy drawn from the battery of the new prosthesis, subject to the kinematic and dynamic constraints. Particle swarm optimization (PSO) is used as the optimization algorithm. A discrete-time PID controller is used to represent the saved energy by means of mass optimization. Optimization illustrated that energy consumption in the batteries can be reduced 51% and provides 1.89 h of additional battery lifetime, according to the literature, by optimizing prosthetic link masses while providing acceptable prosthesis stiffness.

**Keywords:** above-knee prosthesis; robotic; energy minimization; particle swarm optimization; discrete-time model; PID controller; battery life

check for updates

**Citation:** Ege, M.; Kucuk, S. Energy Minimization of New Robotic-Type Above-Knee Prosthesis for Higher Battery Lifetime. *Appl. Sci.* **2023**, *13*, 3868. https://doi.org/10.3390/app13063868

Academic Editor: Salvatore Pasta

Received: 24 February 2023
Revised: 13 March 2023
Accepted: 15 March 2023
Published: 17 March 2023



## 1. Introduction

There are millions of people in the world who have lost their limbs for various reasons, such as accidents, vascular disease including diabetes, peripheral arterial diseases, trauma, and cancer [1]. This situation negatively affects the quality of life and psychology of amputees. Prostheses are of great importance for people with limb losses. A prosthesis may provide both good prosthetic positioning and natural appearance.

Current lower-limb prostheses are mainly grouped into three categories: (i) passive prostheses, (ii) semi-active prostheses [2,3] and (iii) active prostheses [4–7]. Passive prostheses have only passive mechanical structures; therefore, amputees cannot walk comfortably and aesthetically [4]. These cause high metabolic energy consumption and cannot provide sufficient gait symmetry. An amputee with passive prosthesis spends 60% more metabolic energy compared to that used by a healthy person [8]. At the same time, they are not suitable for long-term usage since they cause irritation on the stump. Passive prostheses are preferred by the amputees due to their lower costs compared to semi-active and active prostheses.

One of the main issues in prosthesis design is the need to ensure acceptable joint stiffness for maintaining motion during the gait phase. In semi-active prosthesis, joint stiffness of the prosthesis is controlled by a microprocessor. This control system is powered by a small-size battery that supplies the sensor and microcontroller only. Semi-active prostheses have better joint stiffness characteristics compared to passive prostheses. At the same time, the metabolic energy consumption of semi-active prostheses decreases compared to that of passive prostheses. However, semiactive prostheses are heavier and more expensive than passive prostheses.

Active prostheses are the new generation of prostheses, designed considering the principles of robotic systems [9]. These types of prostheses control joint angles; thus, they require less metabolic energy than passive and semi-active prostheses. They also provide a natural walking ability to the amputees on an uneven terrain [10]. Each joint of active

prostheses is actuated by an independent DC motor and controlled dynamically by a microprocessor. The whole prosthesis mechanism is powered by a battery. Although this active joint mechanism provides a more aesthetic walking ability to the amputees, DC motors particularly increase the weight of the prostheses. This situation both increases energy consumption in the battery and makes amputees consume more metabolic energy. At this stage, lighter active prosthesis with acceptable joint stiffness is the main issue for designers [7].

There are several studies which have been performed in the literature for minimizing the energy consumption of active- or robotic-type prostheses. Verstraten et al. [11] minimized energy consumption of an ankle prosthesis (only one-axis prosthesis driven by a DC motor). They focused on optimizing the drive-train of the prosthesis and spring stiffness values. Rene et al. [12] reduced the torque and power requirements of the ankle prosthesis during the natural walking. The researchers in studies [10,11] used springs in their prostheses. They analyzed motor peak power and energy values. They compared these values with those of conventional actuators.

Unlike the single-axis active prostheses mentioned above, a new robotic-type three-axes above-knee prosthesis has been designed. Its kinematics and dynamic equations are derived symbolically. Energy consumption in robotic-type active above-knee prosthesis is mainly derived from the required torque at each joint [7,11,13–15]. The dominant part of the torque equation is composed of the link masses. Considering this fact, in this study the link masses of new above-knee prosthesis are optimized for minimizing the electrical energy drawn from the battery subject to the kinematic and dynamic constraints. Kinematic constraints refer to limits of joint angles, velocities and accelerations, whereas dynamic constraints denote joint torque limits and stiffness of the prosthesis. PSO algorithm, which was used successfully in the energy optimization problem [16–18] earlier, is selected as the optimization algorithm. A discrete-time PID controller is used to represent the energy saved by means of the mass optimization.

## 2. Mathematical Model of the Above-Knee Prosthesis

In this section, forward/inverse kinematic and dynamic models and a stiffness analysis of the new robotic-type three-axes above-knee prosthesis are given in detail. Trajectory planning is additionally presented.

### 2.1. Design of the New Above-Knee Prosthesis

Figure 1 illustrates the new robotic-type three-axes above-knee prosthesis. In this new design, there are three active joints mounted on the knee and ankle joints. The $\theta_1$ illustrates the revolute knee joint which performs flexion and extension motion. The other two joints, $\theta_2$ and $\theta_3$, intersect at a common point, performing plantar flexion–dorsiflexion and eversion–inversion motions, respectively. $l_1$, $d_3$ and $m_1$, $m_3$ illustrate the lengths and masses of the limbs, respectively. Since $\theta_2$ and $\theta_3$ move the same limb $d_3$, only $m_3$ is used in for ankle mass.

### 2.2. Forward Kinematic Model

Forward kinematic model of the above-knee prosthesis is obtained by using the well-known Denavit–Hartenberg (DH) convention [19]. According to the coordinate frame assignment illustrated in Figure 1, DH parameters [19] are obtained as in Table 1.

**Table 1.** DH parameters of the new above-knee prosthesis.

| i | $\alpha_{i-1}$ | $a_{i-1}$ | $d_i$ | $\theta_i$ |
|---|---|---|---|---|
| 1 | 0 | 0 | 0 | $\theta_1$ |
| 2 | 0 | $l_1$ | 0 | $\theta_2$ |
| 3 | 90 | 0 | 0 | $\theta_3$ |
| 4 | 0 | $l_3$ | $d_3$ | 0 |

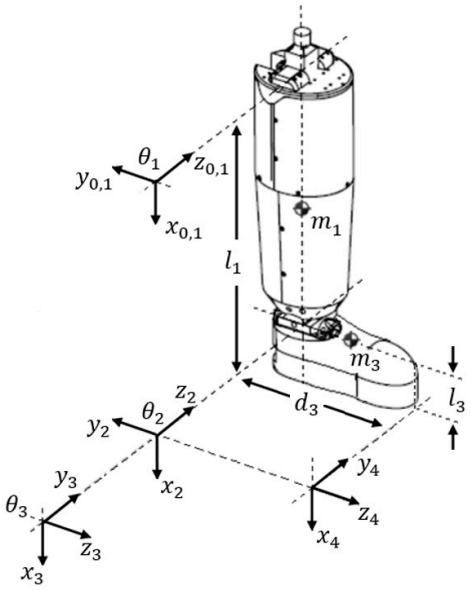


**Figure 1.** The new robotic-type three-axes above-knee prosthesis.

The transformation matrices of the new above-knee prosthesis are obtained as follows.

$$
\begin{aligned}
{}^0_4T &= {}^0_1T\,{}^1_2T\,{}^2_3T\,{}^3_4T \\
{}^0_4T &= \begin{bmatrix} \cos\theta_1 & -\sin\theta_1 & 0 & 0 \\ \sin\theta_1 & \cos\theta_1 & 0 & 0 \\ 0 & 0 & 1 & 0 \\ 0 & 0 & 0 & 1 \end{bmatrix} \begin{bmatrix} \cos\theta_2 & -\sin\theta_2 & 0 & l_1 \\ \sin\theta_2 & \cos\theta_2 & 0 & 0 \\ 0 & 0 & 1 & 0 \\ 0 & 0 & 0 & 1 \end{bmatrix} \begin{bmatrix} \cos\theta_3 & -\sin\theta_3 & 0 & 0 \\ 0 & 0 & -1 & 0 \\ \sin\theta_3 & \cos\theta_3 & 0 & 0 \\ 0 & 0 & 0 & 1 \end{bmatrix} \begin{bmatrix} 1 & 0 & 0 & l_3 \\ 0 & 1 & 0 & 0 \\ 0 & 0 & 1 & d_3 \\ 0 & 0 & 0 & 1 \end{bmatrix}
\end{aligned} \tag{1}
$$

${}^0_4T$ includes the position and orientation of the new above-knee prosthesis in Cartesian space. Performing matrix multiplication in Equation (1) produces

$$
\begin{aligned}
{}^0_4T &= \begin{bmatrix} r_{11} & r_{12} & r_{31} & p_x \\ r_{21} & r_{22} & r_{32} & p_y \\ r_{31} & r_{32} & r_{33} & p_z \\ 0 & 0 & 0 & 1 \end{bmatrix} \\
{}^0_4T &= \begin{bmatrix} \cos\theta_3\cos(\theta_1+\theta_2) & -\sin\theta_3\cos(\theta_1+\theta_2) & \sin(\theta_1+\theta_2) & l_3\cos\theta_3\cos(\theta_1+\theta_2)+l_1\cos\theta_1+d_3\sin(\theta_1+\theta_2) \\ \cos\theta_3\sin(\theta_1+\theta_2) & -\sin\theta_3\sin(\theta_1+\theta_2) & -\cos(\theta_1+\theta_2) & l_3\cos\theta_3\sin(\theta_1+\theta_2)+l_1\sin\theta_1-d_3\cos(\theta_1+\theta_2) \\ \sin\theta_3 & \cos\theta_3 & 0 & l_3\sin\theta_3 \\ 0 & 0 & 0 & 1 \end{bmatrix}
\end{aligned} \tag{2}
$$

### *2.3. Inverse Kinematic Model*

The inverse kinematic model of the new above-knee prosthesis is obtained as follows. Multiplying both sides of Equation (1) by ${}^0_1T^{-1}$ produces the following identity.

$$
\begin{aligned}
{}^0_1T^{-1}\,{}^0_4T &= {}^1_2T\,{}^2_3T\,{}^3_4T \\
\begin{bmatrix} \cos\theta_1 & \sin\theta_1 & 0 & 0 \\ -\sin\theta_1 & \cos\theta_1 & 0 & 0 \\ 0 & 0 & 1 & 0 \\ 0 & 0 & 0 & 1 \end{bmatrix} \begin{bmatrix} r_{11} & r_{12} & r_{13} & p_x \\ r_{21} & r_{22} & r_{23} & p_y \\ r_{31} & r_{32} & r_{33} & p_z \\ 0 & 0 & 0 & 1 \end{bmatrix} &= \begin{bmatrix} \cos\theta_2 & \sin\theta_2 & 0 & l_1 \\ -\sin\theta_2 & \cos\theta_2 & 0 & 0 \\ 0 & 0 & 1 & 0 \\ 0 & 0 & 0 & 1 \end{bmatrix} \begin{bmatrix} \cos\theta_3 & -\sin\theta_3 & 0 & 0 \\ 0 & 0 & -1 & 0 \\ \sin\theta_3 & \cos\theta_3 & 0 & 0 \\ 0 & 0 & 0 & 1 \end{bmatrix} \begin{bmatrix} 1 & 0 & 0 & l_3 \\ 0 & 1 & 0 & 0 \\ 0 & 0 & 1 & d_3 \\ 0 & 0 & 0 & 1 \end{bmatrix}
\end{aligned} \tag{3}
$$

By using Equation (3), $\theta_2, \theta_1$ and $\theta_3$ are obtained as follows.

$$
\theta_2 = A\tan2(A_2, B_2) \pm A\tan2\left(\sqrt{A_2^2 + B_2^2 - C_2^2}, B_2\right) \tag{4}
$$

where $A_2 = 2l_1d_3$, $B_2 = 2l_1l_3\cos\theta_2$, $C_2 = {p_x}^2 + {p_y}^2 - {l_1}^2 - {d_3}^2 - {l_3}^2\cos^2\theta_3$ and $Atan2$ are used for the inverse kinematics of robotic manipulators.

$$\theta_1 = A\tan2(A_1, B_1) \pm A\tan2\left(\sqrt{A_1^2 + B_1^2 - C_1^2}, B_1\right) \tag{5}$$

where $A_1 = p_y$, $B_1 = p_x$, $C_1 = l_1 + d_3\sin\theta_2 + l_3\cos\theta_2\cos\theta_3$

$$\theta_3 = A\tan2\left(\frac{p_z}{l_2}, \sqrt{1 - \left(\frac{p_z}{l_2}\right)^2}\right) \tag{6}$$

### *2.4. Jacobian of the New Above-Knee Prosthesis*

The Jacobian matrix of the above-knee prosthesis is obtained as

$$J = \begin{bmatrix} J_{11} & J_{12} & J_{13} \\ J_{21} & J_{22} & J_{23} \\ 0 & 0 & J_{33} \end{bmatrix} \tag{7}$$

where

$$J_{11} = d_3\cos(\theta_1 + \theta_2) - l_1\sin\theta_1 - l_3\cos\theta_3\sin(\theta_1 + \theta_2) \tag{8}$$

$$J_{12} = d_3\cos(\theta_1 + \theta_2) - l_3\cos\theta_3\sin(\theta_1 + \theta_2) \tag{9}$$

$$J_{13} = -l_3\sin\theta_3\cos(\theta_1 + \theta_2) \tag{10}$$

$$J_{21} = d_3\sin(\theta_1 + \theta_2) + l_1\cos\theta_1 + l_3\cos\theta_3\cos(\theta_1 + \theta_2) \tag{11}$$

$$J_{22} = d_3\sin(\theta_1 + \theta_2) + l_3\cos\theta_3\cos(\theta_1 + \theta_2) \tag{12}$$

$$J_{23} = -l_3\sin\theta_3\sin(\theta_1 + \theta_2) \tag{13}$$

$$J_{33} = l_3\cos\theta_3 \tag{14}$$

### *2.5. Dynamic Model*

The dynamic model of a general serial robotic manipulator can be expressed as

$$\tau = D(\theta)\ddot{\theta} + C(\theta, \dot{\theta}) + G(\theta) + B(\dot{\theta}) \tag{15}$$

where $D$, $C$, $G$ and $B$ illustrate $3 \times 3$ mass matrix, $3 \times 1$ Coriolis/centrifugal force vector, $3 \times 1$ gravity vector and $3 \times 1$ friction, respectively. In this study, $B\left(\dot{\theta}\right)$ is not considered in the dynamic equations. In addition, $\tau, \theta, \dot{\theta}$ and $\ddot{\theta}$ represent torque, position, velocity and acceleration, respectively. The dynamic model of the new above-knee prosthesis is obtained by using Lagrange–Euler method [20] as

$$\begin{bmatrix} \tau_1 \\ \tau_2 \\ \tau_3 \end{bmatrix} = \begin{bmatrix} D_{11} & D_{12} & 0 \\ D_{21} & D_{22} & 0 \\ 0 & 0 & D_{33} \end{bmatrix} \begin{bmatrix} \ddot{\theta}_1 \\ \ddot{\theta}_2 \\ \ddot{\theta}_3 \end{bmatrix} + \begin{bmatrix} C_1(\theta, \dot{\theta}) \\ C_2(\theta, \dot{\theta}) \\ C_3(\theta, \dot{\theta}) \end{bmatrix} + \begin{bmatrix} G_1(\theta) \\ G_2(\theta) \\ G_3(\theta) \end{bmatrix} \tag{16}$$

where $D_{ij}$, $C_i$ and $G_i$ for $i = 1, 2, 3$ & $j = 1, 2, 3$ are given in Appendix A.

### *2.6. Stiffness Analysis*

When the manipulator executes a motion, the end-effector exerts force/moment onto the target. This force/moment causes deflection, which is related to the applied force and the stiffness of manipulator. The stiffness of the serial manipulator directly affects positional accuracy [21]. There are three types of stiffness sources for serial robotic manipulators, namely base, joint and link stiffness. As stated in study [22], the primary source of stiffness

in serial manipulators is the joint stiffness, which is in the axial direction of the actuation torque [22]. The following equation can be written to illustrate the relation between forces and torques.

$$\tau = J^T F \tag{17}$$

where $F(f_x, f_y f_z)$ and $\tau(\tau_1, \tau_2, \tau_3)$ are the $3 \times 1$ vectors of external forces acting on the end-effector of manipulator and actuator forces/torques required to balance these external forces, respectively. The relation between small deflection and joint torques can be stated as follows.

$$\tau = K_\theta \Delta\theta \tag{18}$$

where $K_\theta = diag\begin{bmatrix} k_{\theta_1} & k_{\theta_2} & \cdots k_{\theta_n} \end{bmatrix}$ is the joint stiffness matrix and $\Delta\theta = \begin{bmatrix} \Delta\theta_1 & \Delta\theta_2 & \cdots \Delta\theta_n \end{bmatrix}$ is the small change which occurs in the joint positions. The relation between small change in the end effector $\left(\delta\chi = \begin{bmatrix} \delta x & \delta y & \delta z \end{bmatrix}\right)$ and joint positions can be written as follows.

$$\delta\chi = J\Delta\theta \tag{19}$$

The following equation is obtained by using Equations (17)–(19)

$$\delta\chi = C_x F \tag{20}$$

where $C_x$ is called as compliance matrix and stated as

$$C_x = J K_\theta^{-1} J^T \tag{21}$$

### *2.7. Trajectory Planning*

A fifth-order polynomial is used to compute the joint trajectories of prosthesis proposed in this paper. Coefficients $(s_0, s_1, s_2, s_3, s_4, s_5)$ of the fifth-order polynomial given by Equation (22) can easily be found using Equation (23)

$$\begin{aligned} \theta_i(t) &= s_0 + s_1 t + s_2 t^2 + s_3 t^3 + s_4 t^4 + s_5 t^5 \\ \dot{\theta}_i(t) &= s_1 t + 2s_2 t + 3s_3 t^2 + 4s_4 t^3 + 5s_5 t^4 \\ \ddot{\theta}_i(t) &= 2s_2 + 6s_3 t + 12s_4 t^2 + 20s_5 t^3 \end{aligned} \tag{22}$$

where $i$ = 1, 2 and $n$.

$$\begin{bmatrix} 1 & t_0 & t_0^2 & t_0^3 & t_0^4 & t_0^5 \\ 1 & t_f & t_f^2 & t_f^3 & t_f^4 & t_f^5 \\ 0 & 1 & 2t_0 & 3t_0^2 & 4t_0^3 & 5t_0^4 \\ 0 & 1 & 2t_f & 3t_f^2 & 4t_f^3 & 5t_f^4 \\ 0 & 0 & 1 & 6t_0 & 12t_0^2 & 20t_0^3 \\ 0 & 0 & 1 & 6t_f & 12t_f^2 & 20t_f^3 \end{bmatrix} \begin{bmatrix} s_0 \\ s_1 \\ s_2 \\ s_3 \\ s_4 \\ s_5 \end{bmatrix} = \begin{bmatrix} \theta_0 \\ \theta_f \\ \dot{\theta}_0 \\ \dot{\theta}_f \\ \ddot{\theta}_0 \\ \ddot{\theta}_f \end{bmatrix} \tag{23}$$

Velocity and acceleration of the prosthetic leg in each gait cycle are assumed to be zero at start and rest points. The duration of the gait cycle is selected as 2.52 s. Considering these initial/final conditions and duration ($t$ = 2.52), joint trajectories of a three-axes above-knee prosthesis for a gait cycle is found with simulation. This is shown in Figure 2 where $\theta_i$, $\dot{\theta}_i$ and $\ddot{\theta}_i$ illustrate the position, velocity and acceleration profiles in each gait cycle, respectively.

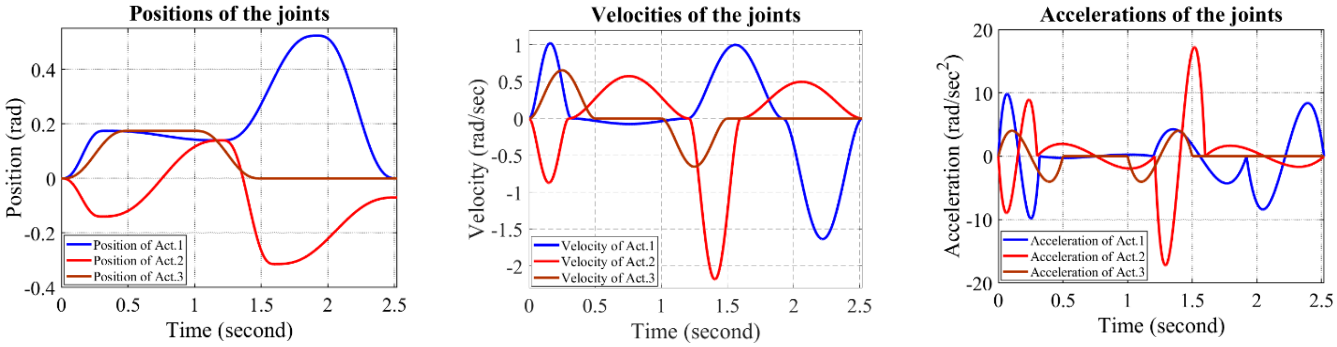


**Figure 2.** Joints trajectories for a gait cycle.

## 3. Experimental Setup

The experimental setup shown in Figure 3 was designed for testing the prosthetic leg mounted from the femoral region. The joint motions were driven by DC motors, where the knee joint performs in one-axis rotation (flexion–extension) and the ankle joint performs in two-axes rotation (plantar–dorsal flexion and eversion–inversion).

**Figure 3.** Experimental setup of the prosthesis.

The minimum and maximum position values of each joint, given in Table 2, were obtained from the experimental setup shown in Figure 3. In addition, the position values of the joints along the trajectory for a gait cycle were obtained by the application of position, velocity and acceleration profiles shown in Figure 2.

**Table 2.** Minimum and maximum values of the kinematic and dynamic parameters for a gait cycle.

| Joints | $\theta_i$ (rad) | | $\dot{\theta}_i$ (rad/sec) | | $\ddot{\theta}_i$ (rad/sec$^2$) | | $\tau_i$ (Nm) | |
|---|---|---|---|---|---|---|---|---|
| | Min | Max | Min | Max | Min | Max | Min | Max |
| 1 | 0 | 0.58 | 0 | 1.65 | 0 | 9.95 | 0 | 7.50 |
| 2 | −0.32 | 0.15 | 0 | 2.85 | 0 | 16 | 0 | 7.50 |
| 3 | 0 | 0.18 | 0 | 0.65 | 0 | 4.5 | 0 | 7.50 |

## 4. Particle Swarm Optimization

The PSO algorithm was first introduced by J. Kennedy and R. C. Eberhart [23] in 1995. This algorithm has proven to be very effective in finding optimal solutions to a wide variety of optimization issues [24,25]. It has shown success, particularly for dynamic optimization issues involving multi-dimensional search spaces [26–28]. When compared to other evolutionary algorithms, it is faster and more efficient at producing robust answers to issues of greater dimensionality that involve continuous nonlinear optimization [29]. PSO mimics behaviors of swarming, such as bird flocking and fish schooling. A population composed of particles is called a swarm. Each particle in a swarm changes its own position according to previous experience to occupy the best position. PSO algorithm is initialized by creating a swarm consists of random particles that search the best value. All particles are compared with the best particles in the previous generation. If it is better than the best particle in the previous generation, this particle is set as the personal best (pbest). The best of pbests is set as the global best (gbest) by comparing the pbests of particles. The positions and velocities of the particles are computed by using following formula.

$$v_{k+1}^i = \omega_k v_k^i + c_1 r_1 (p_k^p - x_k^i) + c_2 r_2 (p_k^g - x_k^i) x_{k+1}^i = x_k^i + v_{k+1}^i \quad (24)$$

where $v_{k+1}^i$ and $x_{k+1}^i$ denote the particles velocity and position, respectively. $\omega_k$ is the inertia weight, $k$ is the current time step and $i$ is the particle number. $c_1$ and $c_2$. selected as 2.05, are the positive acceleration constants. $r_1$ and $r_2$ are random numbers between 0 and 1. The flowchart of the PSO algorithm is given in Figure 4.

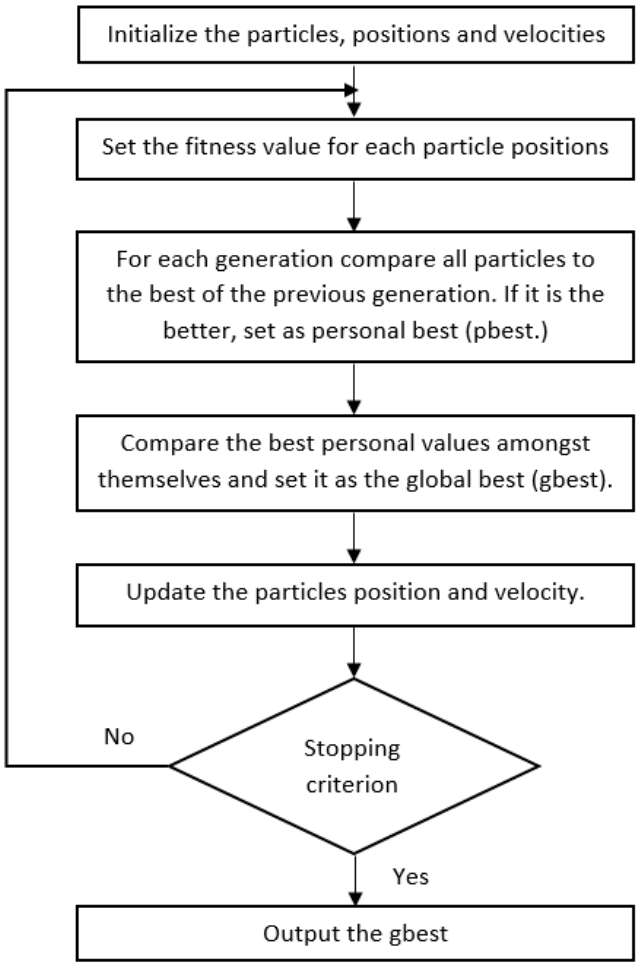


**Figure 4.** Flowchart of PSO algorithm.

## 5. Optimization Objectives

Battery life strictly depends on actuator power consumption which is considered as the optimization objective. Electrical energy consumption E for each actuator of prosthesis is computed as

$$E = \int_0^t P_T dt \tag{25}$$

where $t$ is the total trajectory time and $P_T$ denotes the instantaneous electrical power during a gait cycle. The electrical power is stated as

$$P_T = P_R + P_L + P_E = R_a I_a^2 + L_a I_a \frac{dI_a}{dt} + V_e I_a \tag{26}$$

where $P_R$, $P_L$ and $P_E$ are the resistive power loss, inductive power loss and the power generating the electromotive force, respectively. $P_T$ is the summation of these powers [18,30]. The electrical energy consumed by the three actuators of the prosthesis can be computed as

$$E_T = \sum_{i=1}^{3} E_i \quad \text{i= 1, 2 and 3} \tag{27}$$

## 6. The Statement of the Optimization Problem

The optimization problem of the robotic-type three-axes above-knee prosthesis may be stated as the computation of limb masses to minimize the electrical energy consumed by the joint actuators, subject to kinematic and dynamic constraints.

Min $E_T = \sum_{i=1}^{3} E_i$ $\qquad i = 1, 2$ and 3

Subject to

$\theta_{i,min} \le \theta_i \le \theta_{i,max}$

$\dot{\theta}_{i,min} \le \dot{\theta}_i \le \dot{\theta}_{i,max}$

$\ddot{\theta}_{i,min} \le \ddot{\theta}_i \le \ddot{\theta}_{i,max}$

$m_i \le m_{i,max}$

$\tau_i \le \tau_{i,max}$

$\delta\chi \le \delta\chi_{max}$

where $\theta_{i,min}, \dot{\theta}_{i,min}, \ddot{\theta}_{i,min}$ and $\theta_{i,max}, \dot{\theta}_{i,max}, \ddot{\theta}_{i,max}$ show the position, velocity and acceleration limits of the joints in a gait cycle, respectively. In this study, the numerical values of $\theta_{i,min}, \dot{\theta}_{i,min}, \ddot{\theta}_{i,min}$ and $\theta_{i,max}, \dot{\theta}_{i,max}, \ddot{\theta}_{i,max}$ given in Table 2 are computed considering the limit values of the position, velocity and acceleration profiles in Figure 2. The $m_{i,max}$ illustrates the upper bounds of links masses. The maximum torque values $(\tau_{i,max})$ are computed by substituting the maximum position, velocity and acceleration values in Figure 2 into the dynamic equations of the prothesis. $\delta\chi$ shows the maximum allowable position error for a gait cycle.

The prosthesis is produced with additive manufacturing technology using PLA material. Mass values belonging to each link of the prosthesis and given in Table 3 are obtained by considering the infill pattern and infill density, which vary between 50% and 100%. The link masses in Table 3 are computed by using Cura software program.

There are several types of infill pattern for 3D printing such as grid, lines, triangles, tri-hexagon, cubic, cubic subdivision, octet, quarter-cubic, concentric, zig-zag, cross, cross 3D and gyroid. These patterns are chosen according to the material and its application [31]. Generally, grid, triangles and cubic pattern types are preferred. A grid pattern has a grid-shaped hollow structure and less complex pattern compared to the other two pattern types. A triangle pattern is composed of a 2D mesh made from triangles and has an inherent advantage in strength. A cubic pattern is a 3D pattern of stacked and tilted cubes. This pattern type allows the generation of a high-strength structure. In this study, the grid pattern is used for computing link masses.

**Table 3.** Link mass values considering infill density and pattern of the prosthesis shell structure.

| Infill Density (%) | $m_1$ (gram) | | | | $m_3$ (gram) | | | |
|---|---|---|---|---|---|---|---|---|
| | Triangles | Grid | Cubic | | Triangles | Grid | Cubic | |
| 50 | 2943 | 2871 | 2957 | $(m_{1,min})$ | 1118 | 1041 | 1231 | $(m_{3,min})$ |
| 52 | 2951 | 2880 | 2964 | | 1125 | 1050 | 1238 | |
| 54 | 2960 | 2889 | 2972 | | 1135 | 1058 | 1243 | |
| 56 | 2968 | 2897 | 2981 | | 1142 | 1066 | 1254 | |
| 58 | 2959 | 2904 | 2988 | | 1148 | 1071 | 1259 | |
| 60 | 2965 | 2910 | 2997 | | 1153 | 1080 | 1261 | |
| 62 | 3006 | 2996 | 3005 | | 1259 | 1258 | 1368 | |
| 64 | 3013 | 3005 | 3017 | | 1264 | 1266 | 1376 | |
| 66 | 3023 | 3014 | 3026 | | 1273 | 1271 | 1384 | |
| 68 | 3031 | 3021 | 3034 | | 1281 | 1279 | 1391 | |
| 70 | 3039 | 3028 | 3041 | | 1289 | 1287 | 1395 | |
| 72 | 3048 | 3038 | 3050 | | 1292 | 1292 | 1399 | |
| 74 | 3057 | 3046 | 3058 | | 1299 | 1298 | 1407 | |
| 76 | 3066 | 3056 | 3066 | | 1311 | 1306 | 1415 | |
| 78 | 3074 | 3065 | 3077 | | 1318 | 1314 | 1420 | |
| 80 | 3083 | 3073 | 3086 | | 1325 | 1325 | 1429 | |
| 82 | 3091 | 3081 | 3093 | | 1329 | 1332 | 1435 | |
| 84 | 3100 | 3090 | 3102 | | 1332 | 1339 | 1440 | |
| 86 | 3108 | 3098 | 3110 | | 1346 | 1348 | 1446 | |
| 88 | 3115 | 3107 | 3120 | | 1354 | 1354 | 1453 | |
| 90 | 3126 | 3115 | 3128 | | 1363 | 1360 | 1462 | |
| 92 | 3133 | 3125 | 3136 | | 1369 | 1365 | 1468 | |
| 94 | 3144 | 3133 | 3145 | | 1376 | 1371 | 1474 | |
| 96 | 3151 | 3141 | 3154 | | 1382 | 1378 | 1485 | |
| 98 | 3159 | 3148 | 3162 | | 1388 | 1386 | 1494 | |
| 100 | 3290 | 3179 | 3180 | $(m_{1,max})$ | 1416 | 1406 | 1506 | $(m_{3,max})$ |

The stiffness coefficients of the links $(k_{\theta_1}, k_{\theta_2}, k_{\theta_3})$ are directly affected by the infill density and pattern of the material. Therefore, the stiffness coefficients $(k_{\theta_1}, k_{\theta_2}, k_{\theta_3})$ of links given in Table 4 are computed by using the data in Table 3. Note that the second and third joints correspond to the same mass $(m_2 = m_3)$.

A discrete-time control scheme, illustrated in Figure 5, is used for computing the energy consumption in the actuators. In Figure 5, mm1 and mm2 illustrate the masses of the prosthesis obtained from Table 3. A discrete-time control scheme, composed of a discrete-time PID controller and discrete-time motor model, is shown in Figure 6. The inside of the discrete-time motor model is also illustrated in Figure 7.

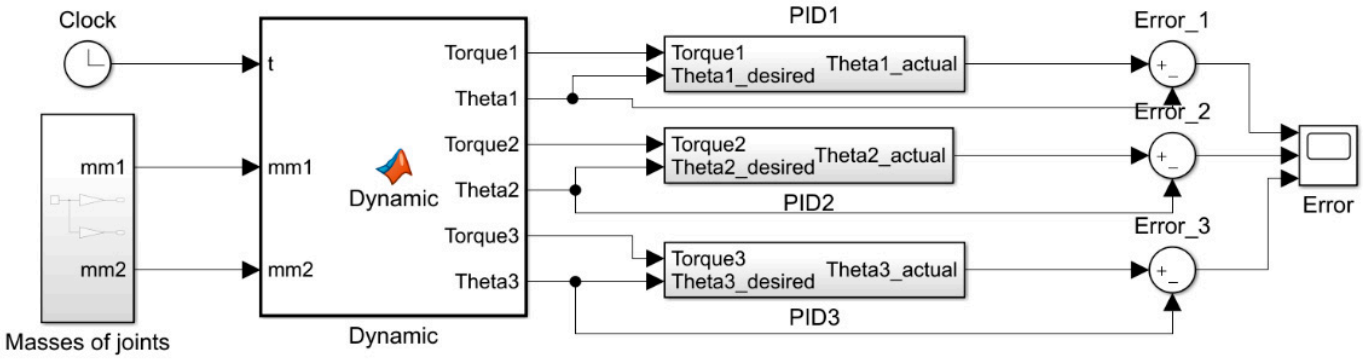


**Figure 5.** A discrete-time control scheme.

**Table 4.** Stiffness coefficients of masses obtained from Cura software (version:4.11.0) program considering infill density and Grid pattern.

| Infill Density (%) | $k_{\theta_1}$ (Nm/rad) | $k_{\theta_2}$ (Nm/rad) | $k_{\theta_3}$ (Nm/rad) |
|---|---|---|---|
| 50 | 101,420 | 101,420 | 101,420 |
| 52 | 101,523 | 101,523 | 101,523 |
| 54 | 101,833 | 101,833 | 101,833 |
| 56 | 101,937 | 101,937 | 101,937 |
| 58 | 102,459 | 102,459 | 102,459 |
| 60 | 107,875 | 107,875 | 107,875 |
| 62 | 110,132 | 110,132 | 110,132 |
| 64 | 110,988 | 110,988 | 110,988 |
| 66 | 112,233 | 112,233 | 112,233 |
| 68 | 113,250 | 113,250 | 113,250 |
| 70 | 114,155 | 114,155 | 114,155 |
| 72 | 115,741 | 115,741 | 115,741 |
| 74 | 116,311 | 116,311 | 116,311 |
| 76 | 117,509 | 117,509 | 117,509 |
| 78 | 118,214 | 118,214 | 118,214 |
| 80 | 119,190 | 119,190 | 119,190 |
| 82 | 121,016 | 121,016 | 121,016 |
| 84 | 122,399 | 122,399 | 122,399 |
| 86 | 123,709 | 123,709 | 123,709 |
| 88 | 124,533 | 124,533 | 124,533 |
| 90 | 126,543 | 126,543 | 126,543 |
| 92 | 127,819 | 127,819 | 127,819 |
| 94 | 129,534 | 129,534 | 129,534 |
| 96 | 136,240 | 136,240 | 136,240 |
| 98 | 144,092 | 144,092 | 144,092 |
| 100 | 155,763 | 155,763 | 155,763 |

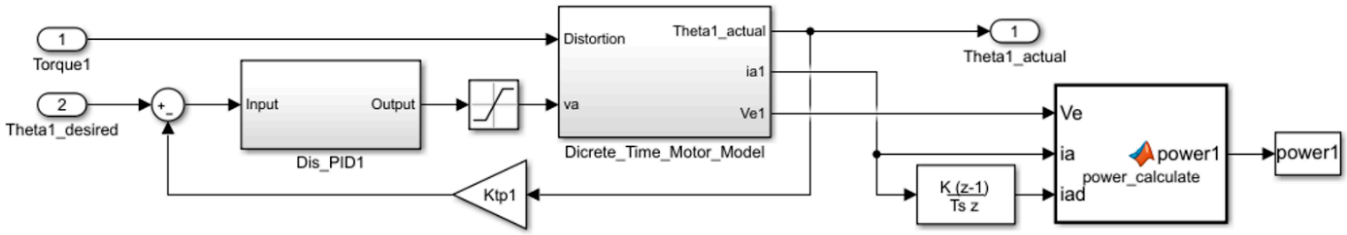


**Figure 6.** Discrete-time PID controller with power computation block.

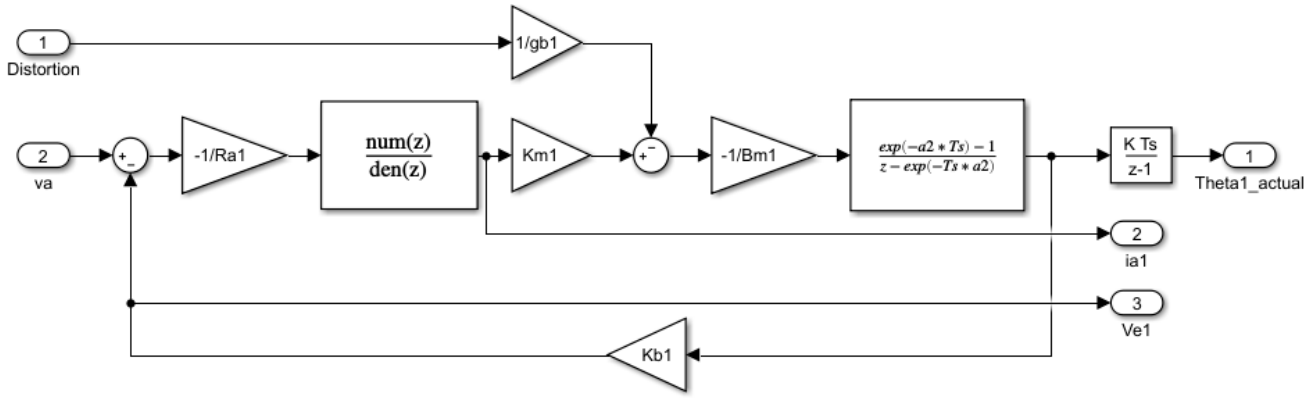


**Figure 7.** Discrete-time motor model.

As can be seen in Figure 6, joint torques are applied to the discrete-time motor model as distributions. The output of the PID block is applied to the discrete-time motor model as voltage (va). There are three outputs of discrete-time motor models, namely $i_a$ (current

drawn by the active actuators), $V_e$ (motor electromotive potential) and Theta_actual (actual position of the joint). $i_{ad}$ denotes the time derivative of the current. In the "power calculate" block, power consumption is computed by using Equation (26). The first two joints, $\theta_1$ and $\theta_2$, are considered to be driven by two identical 7.5 Nm DC motors and the third joint $\theta_3$ is considered to be driven by the 5.4 Nm DC motor. The specifications of all motors are given in Table 5.

**Table 5.** Parameters of DC Motors.

| Parameters | Symbol | Value | Units |
|---|---|---|---|
| Rotor Inertia | Jm | $96.6 \times 10^{-7}$ | $kgm^2$ |
| Armature Resistance | Ra | 0.346 | ohm |
| Armature Inductance | La | 0.121 | Henry |
| Torque Constant | Km | $29.3 \times 10^{-3}$ | Nm/A |
| Back EMF Constant | Kb | $1.18 \times 10^{-2}$ | V/rad/s |
| Armature Voltage | Va | 24 | V |
| Gearbox Ratio | gb | 15:1 | |

As can be noted, the link masses are directly related the dimension of the prosthesis and its infill density. In this study, the lower and upper bounds of the link masses are designed by changing the infill density of prosthesis shell between 50% and 100%, respectively. In general, conventional prostheses use a shell, both for protecting the electronic and mechanical parts and for aesthetic purposes. In this new design, in addition to these two important purposes, shell is mainly used for carrying the mass of the amputee. Thus, the electro-mechanical system of the prosthesis is provided against outer strikes.

## 7. Simulation Results

In this section, the PSO algorithm is applied to an energy minimization problem for a three-linked active above-knee prosthesis. The objective of the study is to optimize the link masses of the above-knee prosthesis to achieve minimum energy consumption while having acceptable stiffness characteristics. The masses of the links are computed by using Cura software program, considering the infill density and infill pattern of the PLA material between 50% and 100%. The population size is used as 10 particles and each particle has two elements ($m_1, m_2 = m_3$). Thus, the swarm size becomes $10 \times 7$ elements. The parameters of the PSO algorithm are selected as $\chi$ = 0.76, c1 = c2 = 2.05, as in [32]. PSO algorithm is applied to the objective function for 60 generations according to the trajectory given by Figure 2 and it is repeated ten times.

After performing the optimization, obeying specified criteria, the link masses are obtained as $m_1 = 2910$ g and $m_2 = m_3 = 1080$ g, with the optimal infill rate of 60%. Optimized parameters are used in the discrete-time PID control scheme to illustrate the energy saving by means of mass optimization. Optimized actuator torques are obtained between $-7.44$ Nm and 5.56 Nm along a walking cycle. These values are less than the specified actuator torque value 7.5 Nm which is given in Table 2. Note that this value is also less than the maximum continuous torque (7.5 Nm) of DC motors given by the manufacturer Maxon. Stiffness values are optimized such that displacement errors $(\delta\chi)$ along the $x$, $y$ and $z$-axes are kept smaller than 1 mm when the end-effector is subjected to forces $F = \begin{bmatrix} fx & fy & fz \end{bmatrix} = \begin{bmatrix} 117.68N & 117.68N & 1176.8N \end{bmatrix}$ at each axis , where $1176.8N$ corresponds to a 120 kg amputee weight. Note that the amputee exerts full force in the $z$ direction while he/she exerts 10 percent of full force in the $x$ and $y$ directions.

Acceptable position tracking errors [33] as shown in Figure 8 are obtained from PID control scheme for each actuator. As can be seen from Figure 8, for a gait cycle, the maximum position tracking errors are obtained as $4.4 \times 10^{-3}$ rad for the first actuator, $2.4 \times 10^{-3}$ rad for the second actuator and $0.14 \times 10^{-3}$ rad for third actuator. In addition to joint tracking errors, Cartesian tracking errors are also demonstrated in Figure 9. The maximum error in Cartesian space is obtained as 1.6 mm for a gait cycle.

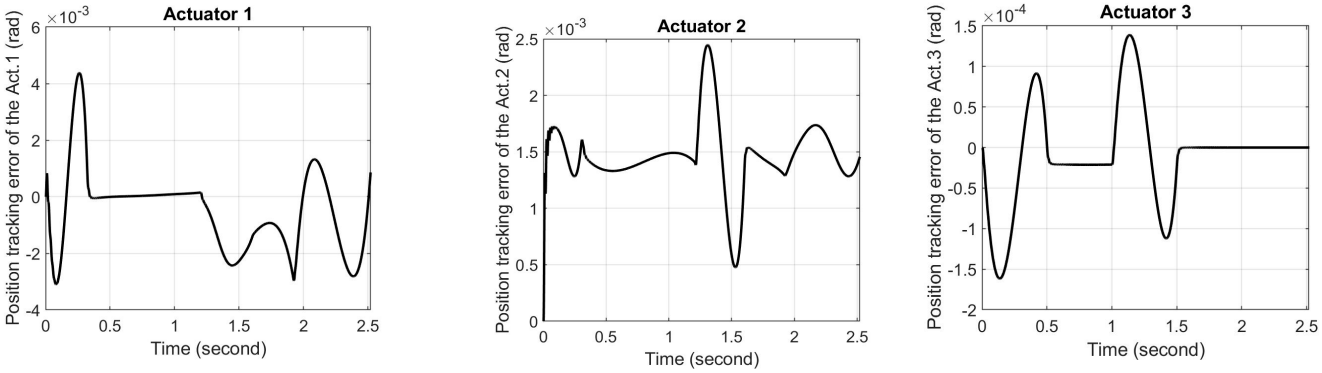


**Figure 8.** Position tracking errors of the joint actuators for a gait cycle.

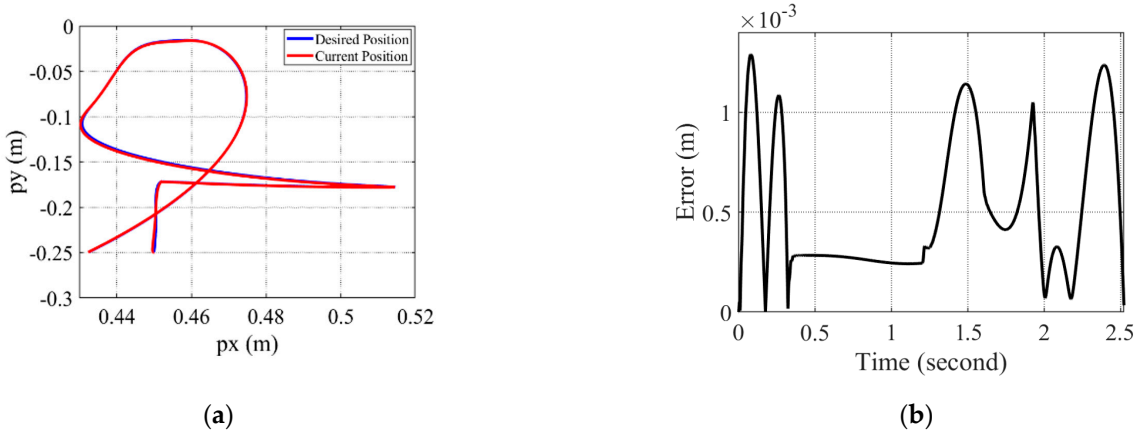


(**a**) (**b**)

**Figure 9.** Cartesian tracking errors: (**a**) Cartesian position; (**b**) Cartesian error.

Figure 10 demonstrates each actuator torque. Maximum torques are obtained as 7.44 Nm for the first actuator, 3.28 Nm for the second actuator and 0.06 Nm for the third actuator. Figure 11 shows the power consumption values consumed by the three actuators. The average power consumptions are obtained as 17 W for the first actuator, 15.07 W for the second actuator and 0.02 W for the third actuator. It should be noted that although the third joint have power consumptions with small variations, the power consumed by the first and second actuators sometimes goes up to 1800 W and 2900 W due to the sudden increase in the load during the gait cycle. The change of joint positions causes these peaks which are normal values in a gait cycle.

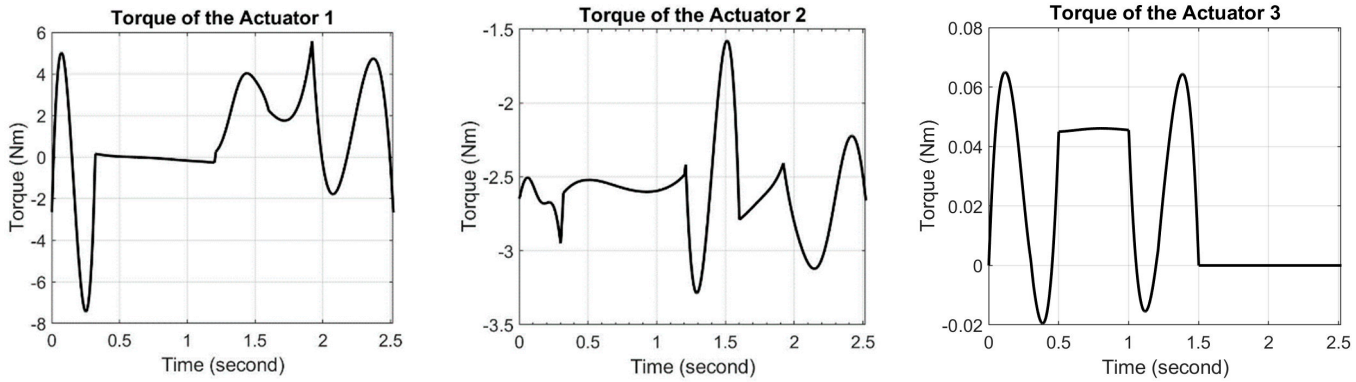


**Figure 10.** Joint torques for a gait cycle.

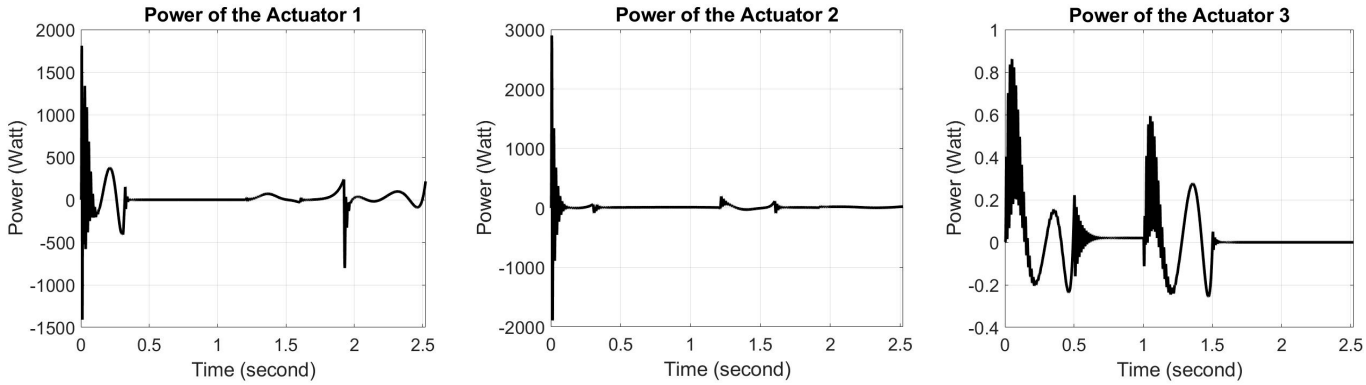


**Figure 11.** Power consumptions of the actuators for a gait cycle.

Power consumptions of three actuators used in above-knee prosthesis are also illustrated as a table (Table 6). Power consumptions of the three actuators are computed for minimum, maximum and optimized mass values.

**Table 6.** Power consumption of three actuators of above-knee prosthesis.

| Consumed Powers | Actuator 1 (Watt) | Actuator 2 (Watt) | Actuator 3 (Watt) | Total (Watt) |
|---|---|---|---|---|
| Minimum power | 16.25 | 14.03 | 0.02 | 30.30 |
| Maximum power | 23.78 | 25.21 | 0.03 | 49.02 |
| Optimized power | 17 | 15.07 | 0.02 | 32.07 |

The optimized stiffness values produce acceptable displacement errors [34] along the $x$, $y$ and $z$ axes. The maximum displacement errors obtained from this study are as follows: 0.7394 mm along the $x$ axis, 0.7392 mm along the $y$ axis and 0.0274 mm along the $z$ axis. The displacement errors along the whole walking cycle are shown in Figure 12.

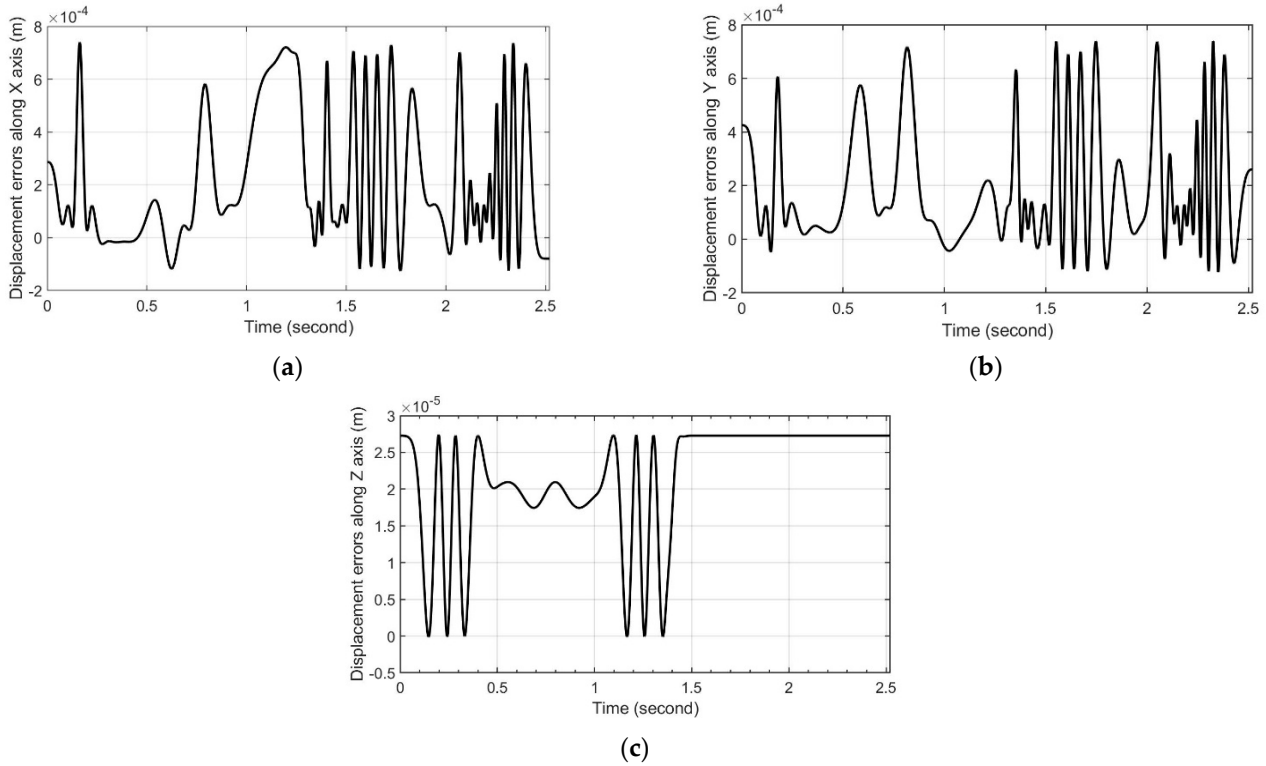


**Figure 12.** Displacement errors along (**a**) $x$ axis (**b**) $y$ axis (**c**) $z$ axis.

## 8. Discussion

Battery life is one of the main challenges in developing an electrically controlled prosthesis. Electrical power consumption directly affects the walking duration of an amputee. The walking comfort of an amputee gets better as the duration of a charge cycle gets longer. The battery life of the above-knee prosthesis presented is computed for three cases, namely minimum prosthesis mass, maximum prosthesis mass and optimized prosthesis mass. The electrical power consumptions and battery life durations obtained in this study are compared to Sup and his colleagues' study [35], which is the only document to give battery results in the current literature. In order to have meaningful results, the same power supply specifications as used in Sup and his colleagues' study are used in the computations. The electrically controlled prosthesis in Sup and his colleagues' study [35] is supplied by a lithium polymer battery with a 29.6 V nominal rating and a 4000 mA·h capacity. Table 7 illustrates power consumptions, gait cycle life and battery life durations of both prostheses. Table 7 also illustrates the minimum and maximum number of steps that a healthy human can generate in one day [36]. As can be seen from Table 7, the new prosthesis proposed in this study consumed about 51% less power than the prosthesis in [35]. As a consequence, the new prothesis proposed in this study provides 1.89 h additional battery life compared to the prothesis in [35]. Considering the step numbers a healthy person will perform in one day [36], the 10,543 steps provided by the new prosthesis illustrate that the new prosthesis presents almost one full day of service with one charge.

**Table 7.** Power consumptions, gait cycle life and battery life durations.

| Studies | Consumed Power in One Cycle (Watt) | Battery Life (Hour) | Gait Cycle Life (Steps) |
|---|---|---|---|
| Results of this paper | 32.07 | 3.69 | 10,543 |
| Sup and colleagues [35] | 66 | 1.8 | 9000 |
| Basset and Tudor-Locke [36] | — | — | 7000–13,000 |

The optimized actuator torques are obtained between −7.44 Nm and 5.56 Nm along a walking cycle. These values are less than the specified actuator torque values 7.5 Nm given in Table 2. Acceptable joint and Cartesian tracking errors are obtained from the PID control scheme for each actuator.

The link mass limits of the prosthesis are obtained according to the infill density and infill pattern of PLA material given by Table 3. Although there are several infill patterns for 3D printing, the grid pattern type is chosen in this study. Since the stiffness coefficients of the links ($k_{\theta_1}, k_{\theta_2}, k_{\theta_3}$) are directly affected by the infill density and infill pattern of the PLA material, the stiffness coefficients of links are computed by using the data in Table 3. Simulations have been performed at the optimal infill rate of 60%. According to the simulations, the link masses are optimized as $m_1 = 2910$ g and $m_2 = m_3 = 1080$ g. Thus, the total mass of the prosthesis is obtained as 3.99 kg. Considering the mass (3.99 kg) and the duration of a walking cycle (2.52 s), total consumed power is obtained as 32.07 W.

## 9. Conclusions

Energy consumption is one of the most important issues for above-knee prosthesis since an amputee desires to use her/his prosthesis for as long as possible. The long-term usage of an electrically controlled above-knee prosthesis mostly depends on the energy consumption of the batteries. Although increasing the number of joints offers comfort and aesthetic walking ability to the amputees, it also increases energy consumption at the battery. Electrical energy supplied by the battery should be carefully consumed for long-term usage. Considering this fact, in this paper, link mass optimization of the new above-knee prosthesis is performed for minimizing the electrical energy consumption while providing acceptable prosthesis stiffness. The PSO algorithm is used as the optimization

algorithm. A discrete-time PID controller is used for representing the energy saved by means of mass optimization.

As a result, the battery life is determined as 3.69 h, corresponding to 10,543 steps in one battery charge. Considering the data in Table 7, the new prosthesis proposed in this study provides almost one full day of service in one charge. Another important remark is that the new prosthesis proposed in this study consumes about 51% less power than the prosthesis developed by Sup and his colleagues [35]. Thus, the new prosthesis provides 1.89 h of additional battery lifetime compared to the prosthesis developed by Sup and his colleagues [35].

The optimized stiffness values provide less than 1 mm displacement errors ($\delta\chi$) along the $x$, $y$ and $z$ axes. This displacement error, determined with the stepping pressure of a 120 kg weight of an amputee, can provide aesthetical movement and balance with acceptable accuracy. In conclusion, the proposed above-knee prosthesis can provide acceptable stiffness performance and almost one full day of walking service in one charge cycle for an amputee under 120 kg weight.

The future studies of this research will include the results of different types of algorithms and controlling strategies by using experimental setup and testing on amputee for different environmental conditions. In addition, new designs can be worked on by considering hip amputation for lower-limb amputees.

## 10. Patents

The ankle mechanism of this study is patented by Turkish Patent and Trademark Office, patent number 201723575.

**Author Contributions:** Conceptualization, M.E. and S.K.; methodology, M.E. and S.K.; software, M.E.; formal analysis, M.E. and S.K.; investigation, M.E. and S.K.; writing—original draft preparation, M.E.; writing—review and editing, S.K.; visualization, M.E.; supervision, S.K.; project administration, S.K. All authors have read and agreed to the published version of the manuscript.

**Funding:** This study was supported by The Scientific and Technological Research Council of Turkiye—TUBITAK, grant number 116M322.

**Institutional Review Board Statement:** Not applicable.

**Informed Consent Statement:** Not applicable.

**Data Availability Statement:** Not applicable.

**Conflicts of Interest:** The authors declare no conflict of interest.

## Appendix A

$$D_{11} = \tfrac{1}{2}d_3^2 m_3 + \tfrac{1}{4}l_1^2 m_1 + 2l_1^2 m_3 + I_{xx_3} + I_{zz_1} + I_{zz_2} - \cos^2\theta_3 I_{xx_3} + \cos^2\theta_3 I_{yy_3} + \tfrac{1}{4}l_3^2 m_3 \cos^2\theta_3 + 2d_3 l_1 m_3 \sin\theta_2 + l_1 l_3 m_3 \cos\theta_2 \cos\theta_3 \quad \text{(A1)}$$

$$D_{12} = D_{21} = \tfrac{1}{2}d_3^2 m_3 + I_{xx_3} + I_{zz_2} - \cos^2\theta_3 I_{xx_3} + \cos^2\theta_3 I_{yy_3} + \tfrac{1}{4}l_3^2 m_3 \cos^2\theta_3 + d_3 l_1 m_3 \sin\theta_2 + \tfrac{1}{2}l_1 l_3 m_3 \cos\theta_2 \cos\theta_3 \quad \text{(A2)}$$

$$D_{13} = -\frac{1}{4}l_3 m_3 (d_3 \sin\theta_3 - l_1 \cos(\theta_2 + \theta_3) + l_1 \cos(\theta_2 - \theta_3)) \quad \text{(A3)}$$

$$D_{21} = \tfrac{1}{2}d_3^2 m_3 + I_{xx_3} + I_{zz_2} - \cos^2\theta_3 I_{xx_3} + \cos^2\theta_3 I_{yy_3} + \tfrac{1}{4}l_3^2 m_3 \cos^2\theta_3 + d_3 l_1 m_3 \sin\theta_2 + \tfrac{1}{2}l_1 l_3 m_3 \cos\theta_2 \cos\theta_3 \quad \text{(A4)}$$

$$D_{22} = \tfrac{1}{2}d_3^2 m_3 + \tfrac{1}{8}l_3^2 m_3 \cos^2\theta_3 - \tfrac{1}{8}l_3^2 m_3 \sin^2\theta_3 + \tfrac{1}{8}l_3^2 m_3 + I_{yy_3} \cos^2\theta_3 + I_{xx_3} \sin^2\theta_3 + I_{zz_2} \quad \text{(A5)}$$

$$D_{23} = -\frac{1}{4}d_3 l_3 m_3 \sin\theta_3 \tag{A6}$$

$$D_{31} = -\frac{1}{4}d_3 l_3 m_3 \sin\theta_3 - \frac{1}{2}l_1 l_3 m_3 \sin\theta_2 \sin\theta_3 \tag{A7}$$

$$D_{32} = -\frac{1}{4}d_3 l_3 m_3 \sin\theta_3 \tag{A8}$$

$$D_{33} = \frac{1}{4}m_3 l_3^2 + \frac{1}{2}I_{zz_3} + \frac{1}{2}(\cos(2\theta_1 + 2\theta_2))I_{zz_3} \tag{A9}$$

$$C_1 = -\frac{1}{4}m_3 l_1 \dot{\theta}_2 (2\dot{\theta}_1 + \dot{\theta}_2)(l_3 \sin(\theta_2 + \theta_3)) - 4d_3 \cos\theta_2 + l_3 \sin(\theta_2 - \theta_3) \tag{A10}$$

$$C_2 = \frac{1}{4}m_3 l_1 \dot{\theta}_1^2 (l_3 \sin(\theta_2 + \theta_3)) - 4d_3 \cos\theta_2 + l_3 \sin(\theta_2 - \theta_3) \tag{A11}$$

$$\begin{aligned} C_3 = {} & (\sin 2\theta_3)(v_1 + v_2)^2 \left(I_{yy_3} - I_{xx_3}\right) + \tfrac{1}{8}l_3^2 m_3 \sin 2\theta_3 (v_1 + v_2)^2 \\ & + \tfrac{1}{4}l_1 l_3 m_3 v_1^2 \sin(\theta_2 + \theta_3) - \tfrac{1}{4}l_1 l_3 m_3 v_1^2 \sin(\theta_2 - \theta_3) \end{aligned} \tag{A12}$$

$$\begin{aligned} G_1 = {} & g(m_3(l_1 \sin\theta_1 - \tfrac{1}{2}d_3 \cos(\theta_1 + \theta_2) + \tfrac{1}{2}l_3 \sin(\theta_1 + \theta_2)\cos\theta_3) \\ & + m_3(l_1 \sin\theta_1 - \tfrac{1}{2}d_3 \cos(\theta_1 + \theta_2)) + \tfrac{1}{2}l_1 m_1 \sin\theta_1) \end{aligned} \tag{A13}$$

$$G_2 = -g(m_3(\frac{1}{2}d_3 \cos(\theta_1 + \theta_2) - \frac{1}{2}l_3 \sin(\theta_1 + \theta_2)\cos\theta_3) + \frac{1}{2}d_3 m_2 \cos(\theta_1 + \theta_2)) \tag{A14}$$

$$G_3 = \frac{1}{2}g l_3 m_3 \cos(\theta_1 + \theta_2)\sin\theta_3 \tag{A15}$$

## References


1. Metts, R.L. *23068 Disability Issues, Trends and Recommendations for the World Bank Protton*; The World Bank: Washington, DC, USA, 2000.
2. Pillai, M.V.; Kazerooni, H.; Hurwich, A. Design of a semi-active knee-ankle prosthesis. In Proceedings of the 2011 IEEE International Conference on Robotics and Automation, Shanghai, China, 9–13 May 2011; pp. 5293–5300. [CrossRef]
3. Lambrecht, B.G.A.; Kazerooni, H. Design of a semi-active knee prosthesis. In Proceedings of the 2009 IEEE International Conference on Robotics and Automation, Kobe, Japan, 12–17 May 2009; pp. 639–645. [CrossRef]
4. Carlos, W.; Júnior, S.; Aurélio, M.; De Oliveira, V.; Bonvent, J.-J. Conception, design and development of a low-cost intelligent prosthesis for one-sided transfemoral amputees. *Res. Biomed. Eng.* **2015**, *31*, 647. [CrossRef]
5. Kapti, A.O.; Yucenur, M.S. Design and control of an active artificial knee joint. *Mech. Mach. Theory* **2006**, *41*, 1477–1485. [CrossRef]
6. Park, K.; Ahn, H.-J.; Lee, K.-H.; Lee, C.-H. Development and performance verification of a motorized prosthetic leg for stair walking. *Appl. Bionics Biomech.* **2020**, *2020*, 8872362. [CrossRef] [PubMed]
7. Tran, M.; Gabert, L.; Hood, S.; Lenzi, T. A lightweight robotic leg prosthesis replicating the biomechanics of the knee, ankle, and toe joint. *Sci. Robot* **2022**, *7*, eabo3996. [CrossRef] [PubMed]
8. Waters, R.L.; Perry, J.; Antonelli, D.; Hislop, H. Energy cost of walking of amputees: The influence of level of amputation. *J. Bone Joint Surg. Am.* **1976**, *58*, 42–46. [CrossRef] [PubMed]
9. Kulkarni, A.S.; Kulkarni, S.M. Robotic Leg Prosthesis. In Proceedings of the 2017 International Conference on Advanced Mechatronics, Intelligent Manufacture, and Industrial Automation (ICAMIMIA), Surabaya, Indonesia, 12–14 October 2017; pp. 97–103.
10. Shultz, A.H.; Lawson, B.E.; Goldfarb, M. Running with a powered knee and ankle prosthesis. *IEEE Trans. Neural Syst. Rehabil. Eng.* **2015**, *23*, 403–412. [CrossRef] [PubMed]
11. Verstraten, T.; Geeroms, J.; Mathijssen, G.; Convens, B.; Vanderborght, B.; Lefeber, D. Optimizing the power and energy consumption of powered prosthetic ankles with series and parallel elasticity. *Mech. Mach. Theory* **2017**, *116*, 419–432. [CrossRef]
12. Jimenez-Fabian, R.; Geeroms, J.; Flynn, L.; Vanderborght, B.; Lefeber, D. Reduction of the torque requirements of an active ankle prosthesis using a parallel spring. *Rob. Auton. Syst.* **2017**, *92*, 187–196. [CrossRef]

13. Park, J.S. Motion profile planning of repetitive point-to-point control for maximum energy conversion efficiency under acceleration conditions. *Mechatronics* **1996**, *6*, 649–663. [CrossRef]
14. Pellicciari, M.; Berselli, G.; Leali, F.; Vergnano, A. A method for reducing the energy consumption of pick-and-place industrial robots. *Mechatronics* **2013**, *23*, 326–334. [CrossRef]
15. Cherelle, P.; Grosu, V.; Flynn, L.; Junius, K.; Moltedo, M.; Vanderborght, B.; Lefeber, D. The Ankle Mimicking Prosthetic Foot 3—Locking mechanisms, actuator design, control and experiments with an amputee. *Rob. Auton. Syst.* **2017**, *91*, 327–336. [CrossRef]
16. Wu, S.; Pan, G.; Yu, L. Dynamic walking gait designing for biped robot based on particle swarm optimization. In Proceedings of the 2012 International Conference on Control Engineering and Communication Technology, ICCECT 2012, Shenyang, China, 7–9 December 2012; pp. 372–377. [CrossRef]
17. Hanifah, R.A.; Toha, S.F.; Hassan, M.K.; Ahmad, S. Power reduction optimization with swarm based technique in electric power assist steering system. *Energy* **2016**, *102*, 444–452. [CrossRef]
18. Kucuk, S. Energy minimization for 3-RRR fully planar parallel manipulator using particle swarm optimization. *Mech. Mach. Theory* **2013**, *62*, 129–149. [CrossRef]
19. Denavit, J.; Hartenberg, R.S. A kinematic notation for lower-pair mechanisms based on matrices. *J. Appl. Mech.* **1955**, *22*, 215–221. [CrossRef]
20. Schilling, R.J. *Fundamentals of Robotics: Analysis and Control*; Prentice Hall: Hoboken, NJ, USA, 1990; Volume 629.
21. Tsai, L.-W. *Robot Analysis: The Mechanics of Serial and Parallel Manipulators*; John Wiley & Sons: Hoboken, NJ, USA, 1999.
22. Alici, G.; Shirinzadeh, B. Enhanced stiffness modeling, identification and characterization for robot manipulators. *IEEE Trans. Robot.* **2005**, *21*, 554–564. [CrossRef]
23. Eberhart, R.; Kennedy, J. Particle swarm optimization. In Proceedings of the IEEE International Conference on Neural Networks, Perth, Australia, 27 November–1 December 1995; Volume 4, pp. 1942–1948.
24. Wang, B.; Xuan, D.; Zhao, X.; Chen, J.; Lu, C. Dynamic battery equalization scheme of multi-cell lithium-ion battery pack based on PSO and VUFLC. *Int. J. Electr. Power Energy Syst.* **2022**, *136*, 107760. [CrossRef]
25. Poli, R. Analysis of the publications on the applications of particle swarm optimisation. *J. Artif. Evol. Appl.* **2008**, *2008*, 685175. [CrossRef]
26. Shoorehdeli, M.A.; Teshnehlab, M.; Sedigh, A.K. A novel training algorithm in ANFIS structure. In Proceedings of the 2006 American Control Conference, Minneapolis, MN, USA, 14–16 June 2006.
27. Kiranyaz, S.; Pulkkinen, J.; Gabbouj, M. Multi-dimensional particle swarm optimization in dynamic environments. *Expert Syst. Appl.* **2011**, *38*, 2212–2223. [CrossRef]
28. Cortez, R.; Garrido, R.; Mezura-Montes, E. Spectral Richness PSO algorithm for parameter identification of dynamical systems under non-ideal excitation conditions. *Appl. Soft Comput.* **2022**, *128*, 109490. [CrossRef]
29. Srinivas, T.; Madhusudhan, A.K.K.; Manohar, L.; Stephen Pushpagiri, N.M.; Ramanathan, K.C.; Janardhanan, M.; Nielsen, I. Valkyrie—Design and development of gaits for quadruped robot using particle swarm optimization. *Appl. Sci.* **2021**, *11*, 7458. [CrossRef]
30. Ur-Rehman, R.; Caro, S.; Chablat, D.; Wenger, P. Multi-objective path placement optimization of parallel kinematics machines based on energy consumption, shaking forces and maximum actuator torques: Application to the Orthoglide. *Mech. Mach. Theory* **2010**, *45*, 1125–1141. [CrossRef]
31. Bhatt, S.; Joshi, D.; Rakesh, P.K.; Godiyal, A.K. Advances in additive manufacturing processes and their use for the fabrication of lower limb prosthetic devices. *Expert Rev. Med. Devices* **2023**, *20*, 17–27. [CrossRef] [PubMed]
32. Eberhart, R.; Kennedy, J. A new optimizer using particle swarm theory. In Proceedings of the Sixth International Symposium on Micro Machine and Human Science, Nagoya, Japan, 4–6 October 1995; pp. 39–43.
33. Ting, Y.; Tosunoglu, S.; Freeman, R. Torque redistribution methods for fault recovery in redundant serial manipulators. In Proceedings of the 1994 IEEE International Conference on Robotics and Automation, San Diego, CA, USA, 8–13 May 1994; pp. 1396–1401. [CrossRef]
34. Jarrett, C.; McDaid, A.J. Robust control of a cable-driven soft exoskeleton joint for intrinsic human-robot interaction. *IEEE Trans. Neural Syst. Rehabil. Eng.* **2017**, *25*, 976–986. [CrossRef] [PubMed]
35. Sup, F.; Varol, H.A.; Mitchell, J.; Withrow, T.J.; Goldfarb, M. Self-Contained Powered Knee and Ankle Prosthesis: Initial Evaluation on a Transfemoral Amputee. In Proceedings of the 2009 IEEE International Conference on Rehabilitation Robotics, Kyoto, Japan, 23–26 June 2009; pp. 638–644.
36. Bassett, D.; Tudor-Locke, C. How many steps/day are enough? Preliminary pedometer indices for public health. *Sports Med.* **2004**, *34*, 1–8.